Supporting Information

Konijnenberg et al. 10.1073/pnas.1413118111

SI Methods

Chromatofocusing. A Mono P 5/200 GL chromatofocusing column (GE Healthcare) was equilibrated with 20 mL start buffer [25 mM Tris-acetic acid (pH 8.3) at 10 °C, 10 mM NaCl, 0.2% (vol/vol) Triton X-100], and a pregradient was formed by washing the column with 6 mL of elution buffer pH 5.0 [7 mL Polybuffer 74, 3 mL Polybuffer 96, 10 mM NaCl, 0.2% (vol/vol) Triton X-100]. The heteropentamer mixture was desalted before application to the chromatofocusing column by using a NAP-10 column. During elution, 250-μL fractions were collected. The pH of the fractions was determined at 6 °C. The protein content of the peak fractions was determined using a 2D Quant Kit (GE Healthcare) according to the manufacturer's protocol.

Fluorescence Dequenching Assay. Proteins were reconstituted into synthetic liposomes according to Koçer et al. (1). Briefly, azolectin was thawed and sized by extrusion 11 times through a 400-nm filter. The resulting liposomes were destabilized by the addition of Triton X-100. Protein and lipids were mixed at 1:50 weight ratio and incubated for 30 min at 50 °C. Subsequently, self-quenching dye solution [200 mM calcein in 10 mM sodium phosphate (pH 8.0)] was added at a 1:1 volume ratio and supplemented with 6 mg (wet weight) Bio-Beads (SM-2 absorbents; Bio-Rad) per microliter of detergent (10% Triton X-100) used in the sample and lipid preparation. For detergent removal, the sample was incubated overnight (~16 h) at 4 °C under mild agitation. The proteoliposomes were applied to a Sephadex G50 Pharmacia size-exclusion column to remove the free dye. All elution fractions were assayed in a Varian Cary Eclipse fluorometer at an excitation wavelength of 495 nm and the emission recorded at 515 nm. In a standard assay, 3 μL calcein-filled proteoliposomes were diluted into 2.2 mL efflux buffer. At $t = 1$ min, MTSET was added at a final concentration of 1 mM for channel activation. The fluorescence was measured continuously, and the total fluorescence of the sample was determined by dissolving the proteoliposomes with 0.5% (vol/vol) Triton X-100 at $t = 7$ min. The datasets were normalized by using the initial fluorescence of each sample as 0% and the signal after the Triton X-100 addition as 100%. The data were fitted to the exponential plot and the first-order rate constants (k) and SD values for calcein efflux were calculated for each heteropentamer.

Sample Preparation and Native IM-MS. MscL homo- and heteropentamers were produced as described elsewhere (2) and solubilized in detergent at 2× critical micelle concentration. Proteins at 5–20 μM were buffer exchanged (Superdex 200 column) into 100 mM ammonium acetate (pH 6.8) and introduced without further desalting into the mass spectrometer using nanoESI with gold-coated borosilicate capillaries at capillary voltages of 1.2–1.6 kV. Spectra were recorded in positive ion mode on a commercially available traveling wave ion mobility mass spectrometer, SYNAPT G2 HDMS (Waters) with 32-kDa quadrupole and settings optimized for transmission of large complexes. Gas pressures were 6.0, $8.35e^{-3}$, $3.26e^{-2}$, and 1.31 mbar for backing, source, trap, and the ion mobility cell, respectively, and He and IMS cell gas flows were 140 and 60 mL/min, respectively. Critical voltages for intact transmission of the detergent/protein complexes were found to be low sampling and extraction cone voltages (1 and 1 V, respectively), with trap and transfer collision energies (CE) set to 10 and 3.5 V, and the trap cell bias to 35 V, unless otherwise stated.

Homo- and heteropentamer samples were incubated for 5 min at room temperature with the indicated concentrations of MTSET (Affymetrix) before analysis. A series of different incubation times revealed that after 5 min no further opening was observed, which is in good agreement with the fast and specific nature of MTSET binding to cysteine residues. Experimental drift time distributions were subjected to a multiple Gaussian fit routine, to extract conformation specific arrival times. All arrival times obtained by IM-MS were then calibrated against proteins of known cross-section such as cytochrome C, β-lactoglobulin, albumin, alcohol dehydrogenase, and glutamate dehydrogenase, as reported previously to yield CCSs (3). All reported cross-sections are from one of the lowest observed charge states (16+), because it represents the most native conformation. The m/z scale of all mass spectra was externally calibrated using a 10-mg/mL cesium iodide (CsI) solution. The spectra were processed using MassLynx 4.1.

1. Koçer A, Walko M, Feringa BL (2007) Synthesis and utilization of reversible and irreversible light-activated nanovalves derived from the channel protein MscL. *Nat Protoc* 2(6):1426–1437.
2. Birkner JP, Poolman B, Koçer A (2012) Hydrophobic gating of mechanosensitive channel of large conductance evidenced by single-subunit resolution. *Proc Natl Acad Sci USA* 109(32):12944–12949.
3. Bush MF, et al. (2010) Collision cross sections of proteins and their complexes: A calibration framework and database for gas-phase structural biology. *Anal Chem* 82(22):9557–9565.

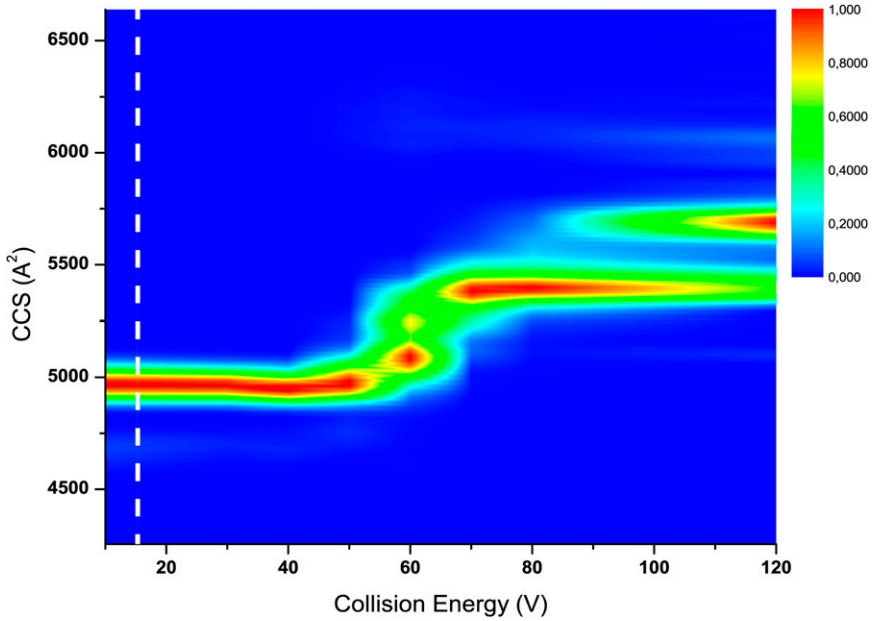

Fig. S1. Collision-induced unfolding of MscL. Heat map representation of collision-induced unfolding of the 16+ charge state of MscL. The internal energy of the protein increases due to more energetic collisions (higher acceleration voltage) with a neutral buffer gas, leading to increasing CCS (unfolding). The dotted white line represents the energy regime used throughout this study.

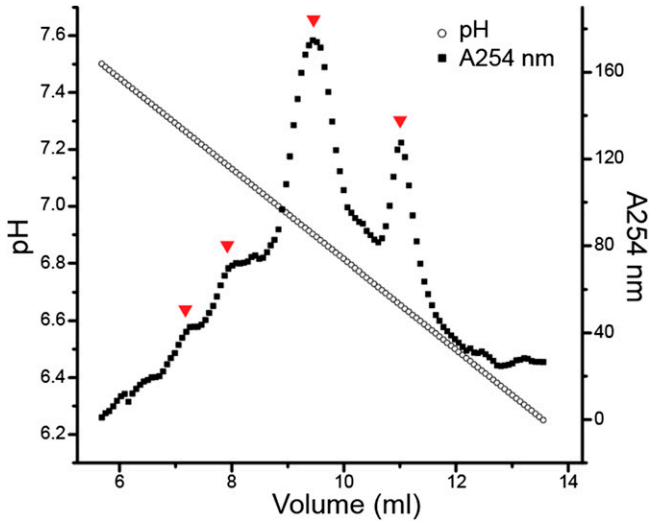

Fig. S2. Chromatofocusing profile. MscL heteropentamers with different numbers of WT-StrepII and G22C-6His subunits differ in their surface isoelectric point (pI). The normalized chromatogram shows four peaks representing the individual populations: WT_1G22C_4, WT_2G22C_3, WT_3G22C_2, and WT_4G22C_1 (from left to right).

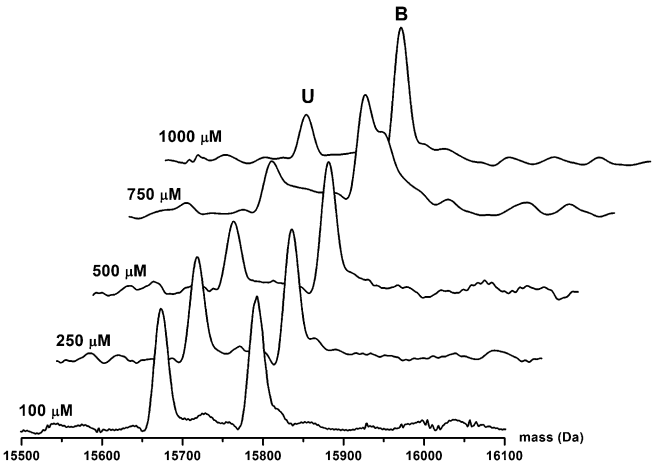

Fig. S3. Titration of $G22C_5$ MscL with MTSET. Covalent MTSET binding was assessed after collision-induced dissociation (70–100 V CE) of the complex in the gas phase because the mass difference induced by MTSET binding was too small to observe in native MS using our current soft release approach, due to peak broadening caused by the polydisperse nature of the detergent that remains bound to the pentamers. The spectra show the overall ratio of MscL subunits with (B) and without (U) MTSET covalently attached. MscL did not seem to be saturated despite the specific nature of MTSET binding to cysteines, although after 750 μM no significant change in the bound vs. unbound ratio was observed. It is possible that further binding of MTSET to the five reactive cysteine sites in the pore lining is somehow limited by the positive charge density that is obtained after MTSET binding to several cysteines.

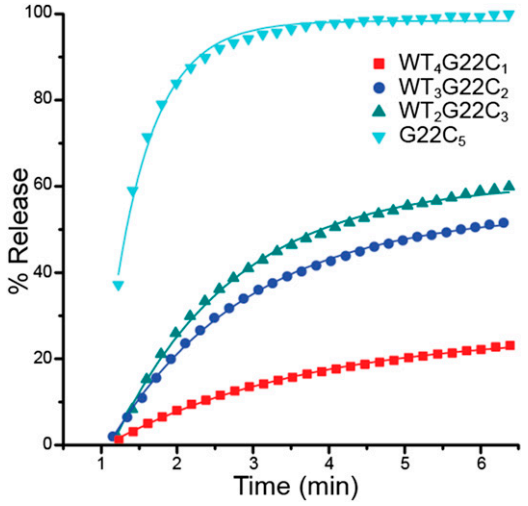

Fig. S4. Fluorescence dequenching assay. Homo- and heteropentamers of MscL were assayed by a fluorescence dequenching assay. The net percent release of liposomal fluorophore content was calculated from the increase in fluorescence after activating the channel with 1 mM final concentration of MTSET. Single exponential efflux rate constants are $kWT_4G22C_1 = 0.38 \pm 0.08\ min^{-1}$, $kWT_3G22C_2 = 0.55 \pm 0.03\ min^{-1}$, $kWT_2G22C_3 = 0.62 \pm 0.04\ min^{-1}$, $kG22C_5 = 1.84 \pm 0.02\ min^{-1}$.

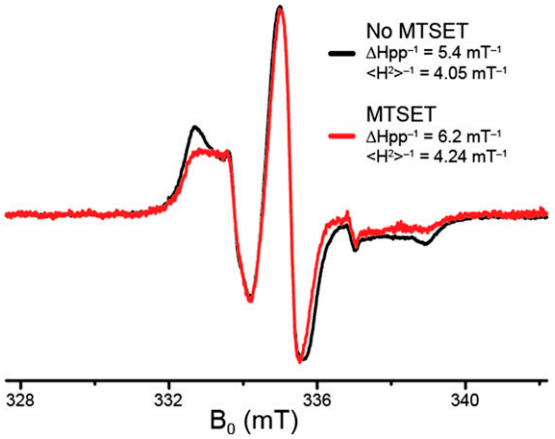

Fig. S5. CW-EPR spectra of spin-labeled G22C MscL solubilized in Triton X-100 at room temperature. MscL was partially labeled at its 22nd amino acid position with a cysteine-specific spin probe MTSSL with the labeling efficiency of 50%. EPR spectra were normalized to maximum amplitude and correspond to 36 accumulations (black trace, no MTSET; red trace, with MTSET; protein concentration 285 μM). Two EPR parameters are used to assess the mobility of the spin probe quantitatively: the mobility parameter (the inverse of the central line width, $_{\Delta}Hpp^{-1}$) and the inverse of the second moment ($<H^2>^{-1}$). An increase in the spin-label motional freedom is reflected in an increase of both numerical values and is associated with channel opening. In the absence of MTSET, the values were $_{\Delta}Hpp^{-1} = 5.4\ mT^{-1}$; $<H^2>^{-1} = 4.05\ mT^{-1}$, whereas in the presence of MTSET: $_{\Delta}Hpp^{-1} = 6.2\ mT^{-1}$; $<H^2>^{-1} = 4.24\ mT^{-1}$. This increase in both EPR parameters indicates that upon MTSET binding, detergent solubilized MscL opens in the absence of a lipid bilayer environment.

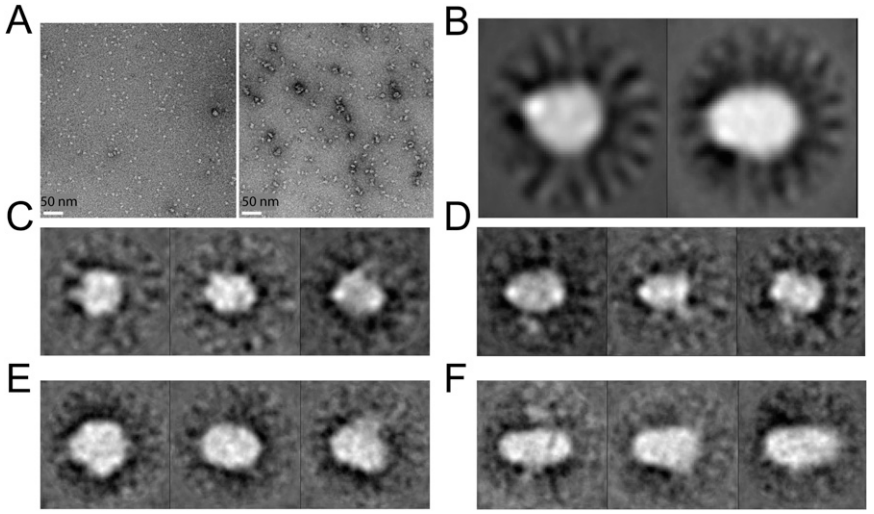

Fig. S6. Electron micrograph and image processing of MscL closed and open states. Closed-state or open-state MscL was applied at a concentration of ∼0.03 mg/mL to electron microscope grids and stained with 2% uranyl acetate. (*A*) Electron micrographs of negatively stained MscL. (*Left*) Closed state. (*Right*) Open state. The particles appear white on a darker background. (*B*) Image averaging of MscL. (*Left*) Image averaging of 1,403 closed-state particles (centered and aligned) (*Right*) Image averaging of 1,004 different partially opened channels (centered and aligned). (*C*–*F*) Gallery from selected classes from classification. (*C* and *D*) Closed-state MscL. (*C*) Three classes showing the top views. (*D*) Three classes showing the side view. (*E* and *F*) Open-state MscL. (*E*) Three classes showing the top view. (*F*) Three classes showing the side view. The size of the box is 212 × 212 Å.

Table S1. Gas-phase detergent cluster stability depends strongly on the ability to form intermolecular hydrogen bonds

		Solution phase			Gas phase		
Detergent name	Detergent type	Aggregation no.*	H-bond donor sites	H-bond acceptor sites	Maximum cluster size, kDa	Maximum aggregation no.	Maximum charge state
DDM	Nonionic	78–149	7	11	60.2	118	10+
Triton X-100	Nonionic	75–165	1	10 avg.	—	6	2+
LDAO	Ionic	76	0	2	—	2	1+

The table presents the gas- and solution-phase characteristics of several detergent micelles used in this study. Detergents were measured (without MscL) at a concentration that equaled 2× the critical micelle concentration and transferred to the gas phase using nanoESI. The stability of detergent clusters ("micelles") in vacuo can be deduced from their cluster sizes in the gas phase under identical, mild desolvation conditions. Detergents that are unable to form extensive intermolecular hydrogen bonds do not display larger clusters in the mass spectra due to the loss of the hydrophobic effect in the gas phase. *Values taken from www.anatrace.com.

Table S2. IM-MS allows for size determination of different homo- and heteropentamers

	Masses		Closed states		Opened states
Species	Theoretical, Da	Observed, Da	CCS, Å^2	CCS, tag corrected, Å^2	CCS, tag corrected and relative abundance, Å^2 %
WT-6His	78,255	78,342 ± 29	4,861 ± 61	—	—
WT-StrepII	79,345	79,461 ± 32	4,927 ± 59	—	—
WT_4G22C_1	79,173	79,182 ± 37	4,944 ± 64	4,959 ± 64	4,952 ± 63 (100%)
WT_3G22C_2	79,001	79,114 ± 45	4,917 ± 59	4,947 ± 59	4,950 ± 62 (47%); 5,266 ± 64 (34%) 5,557 ± 98 (19%)
WT_2G22C_3	78,829	78,882 ± 42	4,902 ± 63	4,948 ± 63	4,965 ± 62 (27%); 5,228 ± 56 (34%) 5,555 ± 68 (38%)
$G22C_5$	78,485	78,600 ± 15	4,884 ± 63	4,960 ± 63	5,095 ± 46 (21%); 5,330 ± 48 (35%) 5,580 ± 56 (29%); 5,890 ± 106 (15%)

Reported CCSs were obtained after a multiple Gaussian curve fit, to obtained conformation-specific arrival times. Reported errors correspond to a 90% valley width of the curve fitted to conformation-specific ion mobility peaks. The small difference in measured CCS of MscL pentamers can be correlated to the difference in purification tags. For comparison of the CCSs from each of the heteropentamers, we performed a small correction on the CCS corresponding to the composition of purification tags to the CCS (denoted as CCS, tag corrected). Reported relative abundances were obtained by comparing the surface areas of the conformation-specific ion mobility peaks.